Journal of Alloys and Compounds 509 (2011) 210–216

Contents lists available at ScienceDirect

Journal of Alloys and Compounds

journal homepage: www.elsevier.com/locate/jallcom

DFT studies of hydrogen storage properties of $Mg_{0.75}Ti_{0.25}$

Shu Xia Tao*, Peter H.L. Notten, Rutger A. van Santen, Antonius P.J. Jansen

Laboratory of Inorganic Chemistry and Catalysis, P.O. Box 513, 5600 MB Eindhoven, The Netherlands

ARTICLE INFO

Article history:
Received 2 June 2010
Received in revised form 9 September 2010
Accepted 18 September 2010
Available online 25 September 2010

Keywords:
Mg–Ti alloy
Hydrogen storage
Hydrogen absorption energy

ABSTRACT

Absorption energies of hydrogen in $Mg_{0.75}Ti_{0.25}$ alloys as a function of the hydrogen concentration were calculated using Density Functional Theory. Four types of structures of alloys and their hydrides including $TiAl_3$, $ZrAl_3$, $AuCu_3$, and segregated types of structures were considered. The stability of the configurations, and the structural and electronic bonding properties were studied. The hydrogenation properties depend highly on the structure of the alloys. The ordered alloys have very similar properties to that of pure Mg. For segregated alloys, the hydrogenation properties can be divided to Ti-like, ordered alloy-like and Mg-like from low to high hydrogen concentration. The formation energies show that for the four structures, segregated $Mg_{0.75}Ti_{0.25}$ is favored for alloys, whereas $TiAl_3$ type of $Mg_{0.75}Ti_{0.25}H_2$ are favored for hydrides. Therefore hydrogen induced structural rearrangement of the intermetallic structures of the $Mg_{0.75}Ti_{0.25}$ might occur upon hydrogen cycling. For the non-homogenous Mg–Ti–H system, further phase segregation of Ti in Mg might occur. Partial dehydrogenation with some hydrogen remaining in the Ti-rich region may improve reversibility.

1. Introduction

Progress in the 20th century in hydrogen storage in Mg-based alloys has been summarized by Schlapbach and Züttel [1]. Kinetics and thermodynamic properties have been improved by alloying Mg with V, Cu, Al, Ni, Fe, Co, Mn and some of their oxides [2–13], but the main challenges, such as high operation temperature and low hydrogen absorption and desorption rates, still remain. Recently, Notten and co-workers [17–20] reported the excellent hydrogen storage capacity of Mg–Ti–H bulk and thin films, which is approximately five times larger than that of conventional metal hydride electrodes in NiMH batteries. Electrochemical measurements have shown that adding Ti positively affects the kinetics of hydride formation compared with MgH_2, which has been related to the transformation from rutile to fluorite of the hydride structure. The improved kinetics is in consistent with several theoretical predictions [14–16]. Also, intriguing optical changes of $Mg_xTi_{1-x}H_{2y}$ as a function of hydrogen concentration, going from absorbing to highly transparent, created new opportunities in, for instance, the field of hydrogen sensing and switchable smart coatings in solar collectors [21–24]. A common property desirable for all applications is the ability of the Mg–Ti alloy to rapidly take up and release hydrogen.

The binary phase diagram of Mg and Ti indicates that no stable bulk compounds are formed. However, based on X-ray diffraction results (XRD) it has been reported that alloying of Mg and Ti does take place in mechanically alloyed bulk samples [25–27] and in thin films by using physical vapor deposition [28], e-beam deposition [19,20], and sputtering [21,29]. Mitlin and co-workers [30,31] reported that hydrogen sorption enhancement in Mg–Ti–Pd system is due to improved kinetics rather than any altered thermodynamics and stable TiH_2 was formed at the Mg surfaces preventing complete Pd–Mg interdiffusion or acting as hydrogen catalyst. Electrochemical measurements revealed that the (de)hydrogenation rate heavily depends on the ratio of Mg and Ti [20,29]. For alloys containing 10 at.% Ti or less the system cannot be (de)hydrogenated rapidly, whereas inserting and extracting hydrogen is greatly facilitated for alloys containing more than 10 at.% Ti. In line with the difference in the ability to insert and extract hydrogen at an appreciable rate the crystal structures of the associated Mg-based hydrides were found to be different. XRD measurements pointed to a face-centered cubic (fcc) structure with excellent kinetics and a body-centered tetragonal (bct) lattice where hydrogen transport was strongly inhibited [32]. The hydride structure transformation from rutile to fluorite by alloying Ti to Mg was also confirmed by earlier DFT calculations [33,34]. The transition point for Mg–Ti hydrides was determined to be around $Mg_{0.8}Ti_{0.2}$. Vermeulen et al. [35] investigated the structural transformations throughout the (de)hydrogenation process. XRD and electrochemical (de)hydrogenation were performed *in situ* to monitor the symmetry of the unit cells of Mg_xTi_{1-x} thin film alloys along the pressure-composition isotherms at room temperature. The lattice spacings found for $Mg_{0.7}Ti_{0.3}H_{2y}$ revealed that the Mg-to-Ti ratio changed continuously in the two phase coexistence region. Since the XRD patterns have ruled out large scale segregation, the results

* Corresponding author.
E-mail address: s.x.tao@tue.nl (S.X. Tao).

0925-8388/$ – see front matter © 2010 Elsevier B.V. All rights reserved.
doi:10.1016/j.jallcom.2010.09.091

implied a nanostructured alloy with Ti-poor and Ti-rich regions in which Mg and Ti atoms were not randomly distributed. In addition, Srinivasan et al. [36] investigated $Mg_{0.65}Ti_{0.35}D_x$ prepared by ball milling and gas-phase deuterium absorption. By combined use of XRD, neutron diffraction, and magic-angle-spinning H nuclear magnetic resonance(NMR), partial segregation structures with rutile MgD_2 domain and interdispersed TiD_y and a separated fcc TiD_z phases were observed. By continuously monitoring the structure during hydrogen uptake, Borsa et al. [23] have obtained data that are compatible with a coherent structure, and they proposed that the average structure resembled rutile MgH_2 at high Mg content and was fluorite otherwise. On the other hand, Baldi et al. [37] investigated $Mg_xTi_{1-x}H_{2y}$ thin film systems by combining XRD and Extended X-ray Absorption Fine Structure (EXAFS) spectroscopy. Despite the positive enthalpy of mixing of Mg and Ti, they found that the degree of ordering did not vary upon loading and unloading with hydrogen. The robustness of this system and the fast and reversible kinetics of (de)hydrogenation were attributed to the formation of nanoscale compositional modulations in the intermetallic alloy. Instead of preparing Mg–Ti alloys, nano-structured Mg–Ti–H from mixing MgH_2 and TiH_2 by ultrahigh-energy-high-pressure mechanical milling have been prepared [38–40]. Lu et al. [39,40] proposed that TiH_2 is uniformly distributed in MgH_2, and not only the kinetics but also the thermodynamics are changing with different MgH_2/TiH_2 ratios and milling conditions. As summarized above, Mg–Ti–H systems made by different experimental approaches show a variety of hydrogen properties.

Thus, an unambiguous confirmation of the structures, thermodynamics, and electronic bonding properties of Mg–Ti–H system is necessary. In our previous paper [41], the hydrogenation properties of pure Ti and Mg were investigated, and we continue to investigate Mg–Ti alloys in this paper. A composition of $Mg_{0.75}Ti_{0.25}$ is chosen because 25 at.% Ti is large enough to obtain the structural transformations according to both experimental [32,35] and theoretical predictions [33]. In addition, the ratio of Mg:Ti = 3:1 allows us to use a relatively small unit cells in the model of the fcc structures.

2. Computational methods and structural models

All calculations were performed using Density Functional Theory as implemented in the Vienna Ab-Initio Simulation Package (VASP) [42,43]. The Kohn-Sham equations were solved using a basis of Projector Augmented Wave-functions with a plane-wave energy cut-off 300 eV [44], and using pseudopotentials [45] to describe the core electrons. The Perdew-Wang 1991 generalized gradient approximation was used for the electron-exchange correlation potential [46]. A total of $13 \times 13 \times 13$ k points were used to model the Brillouin zone for the four metal unit cell structures (see Fig. 1C). With this number of k points, the influence of the distribution of the k points on the calculated total energies became less than 0.02% and therefore this number of k points was deemed sufficiently large. For larger cells k points were scaled down proportionally, e.g. for a lattice parameter of double length, only half number of k points were required. Therefore for sixteen metal atom cells (see Fig. 1A), $13 \times 13 \times 3$ k points were used. For all structures the lattice parameters, the volume and the atom positions were allowed to relax. Mg is non-magnetic and therefore does not require spin-polarized calculations. On the other hand, we have performed spin-polarized calculations for Ti metals and its hydrides in the fluorite structures to estimate the importance of spin polarization on the hydride formation energies. It turned out that the inclusion of spin polarization has no effect on the bulk hydride formation energies.

All models in this paper have a fixed ratio of Mg:Ti = 3:1. Since the energy difference of the hcp and fcc metals is very small and the hcp structure transforms immediately to fcc upon loading of hydrogen [41], a hypothetical metastable fcc structure is assumed for the alloys. Fig. 1 shows the four different structures and their corresponding unit cells used in the calculations. They are $ZrAl_3$ type (A), $TiAl_3$ type (B), $AuCu_3$ type (C) and segregated type (D) $Mg_{0.75}Ti_{0.25}H_2$ with hydrogen atoms in tetrahedral sites.

The hydrogenation processes are described by the following reaction, where Y is the number of hydrogen molecule per metal

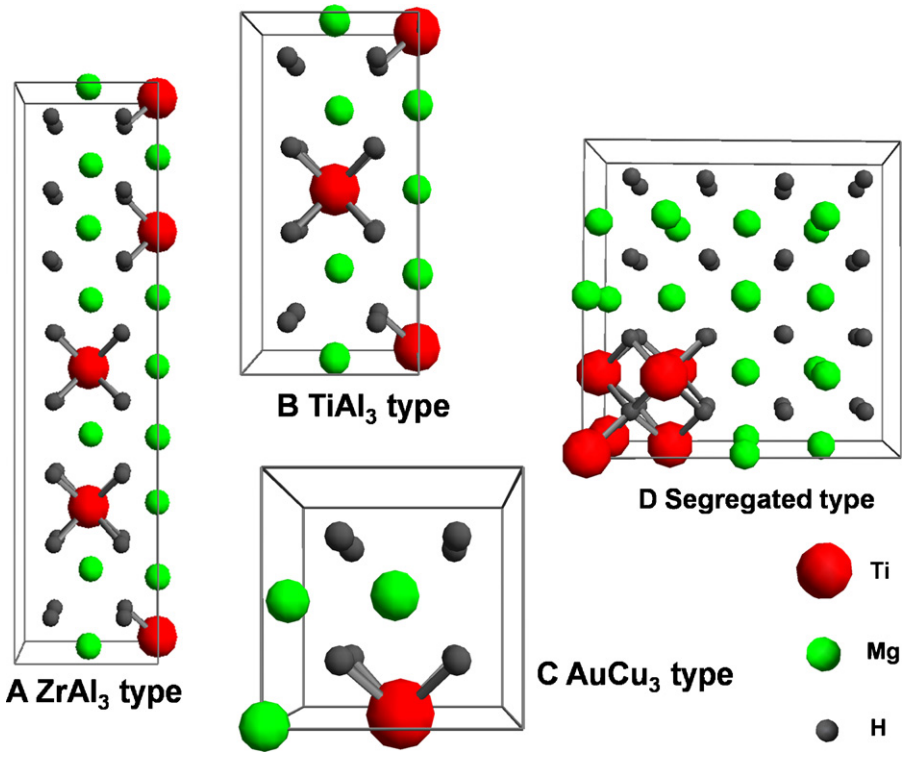

Fig. 1. Unit cells used in the calculations for the three structures.

(for fluorite hydride $Y = 1$, for the fcc alloy $Y = 0$).

$$0.75\mathrm{Mg(hcp)} + 0.25\mathrm{Ti(hcp)} + y\mathrm{H_2} \rightleftharpoons \mathrm{Mg_{0.75}Ti_{0.25}H_{2y}} \quad (1)$$

The formation energy of alloys and hydrides are defined as

$$\Delta E_{\mathrm{M}} = E_{\mathrm{Mg_xTi_{1-x},fcc}} - xE_{\mathrm{Mg,hcp}} - (1-x)E_{\mathrm{Ti,hcp}} \quad (2)$$

$$\Delta E_{\mathrm{H_2}} = \frac{E_{\mathrm{Mg_xTi_{1-x}H_{2y}}} - xE_{\mathrm{Mg,hcp}} - (1-x)E_{\mathrm{Ti,hcp}} - yE_{\mathrm{H_2}}}{y} \quad (3)$$

ΔE_{M} is the formation energy of the alloys or metals with the same structure to their hydrides (in eV/M), whereas $\Delta E_{\mathrm{H_2}}$ is the formation energy of the hydride normalized to the number of H_2 molecules (in eV/H_2). Such normalization is always used to compare the formation energies at different hydrogen concentrations. $E_{\mathrm{H_2}}$, $E_{\mathrm{Mg,hcp}}$ and $E_{\mathrm{Ti,hcp}}$ are the energies of the H_2 molecule and the hcp metal (per metal atom) as obtained from their respective calculations; $E_{\mathrm{Mg_xTi_{1-x}H_{2y}}}$ and $E_{\mathrm{Mg_xTi_{1-x}fcc}}$ are the total energies normalized to the number of metal atoms in the unit cell. The hydrogenation energy of the alloys per H_2 molecule is given by $\Delta E_{\mathrm{H_2}} - \Delta E_{\mathrm{M}}$. The calculation of atomic hydrogen and the molecule H_2 has been done using a cubic supercell with size 10 Å × 10 Å × 10 Å The bond length is predicted to be 0.746 Å and the binding energy 461 kJ/mol H_2. The agreement with the experimental data (0.741 Å and 456 kJ/mol H_2) is satisfactory. A validation of the accuracy for the structural parameters of the metals were made in our previous paper [41]. The agreement with the literature values was fairly good, therefore the details will not be shown here again.

3. Results

In this part, the formation energies as a function of hydrogen concentration of the $ZrAl_3$ type, $TiAl_3$ type, $AuCu_3$ type and segregated type of $Mg_{0.75}Ti_{0.25}H_{2y}$ shown in Fig. 1 are studied, respectively. Comparisons of hydrogenation properties between the four types of alloys, and also those of pure Mg and Ti are made.

3.1. Formation energy as a function of hydrogen concentration

3.1.1. $ZrAl_3$ type, $TiAl_3$ type and $AuCu_3$ type

The formation energy of $ZrAl_3$ type, $TiAl_3$ type and $AuCu_3$ type $Mg_{0.75}Ti_{0.25}$ alloys(ΔE_{M}) are 0.21, 0.19 and 0.14 eV/M, respectively. The positive value means that it is unfavorable to form the structure. The available tetrahedral sites and octahedral sites in these three structures are all identical, i.e. with one Ti and three Mg neighbors for hydrogen in tetrahedral sites or with two Ti and four Mg neighbors in octahedral sites. Distributions of hydrogen atoms over tetrahedral sites, octahedral sites, combination of tetrahedral and octahedral sites were calculated. The energies and structures were analyzed similarly as have been done for fcc Mg and Ti in our previous paper [41].

The hydrogenation properties of these three types of alloys are qualitatively similar to those of fcc Mg. For instance, the most favorable distributions of hydrogen atoms in the metal lattice are the same as that of fcc Mg: (i) tetrahedral sites are always favored over the octahedral sites with hydrogen atoms clustering in the metal lattice, and (ii) lattice distortions occur with increasing hydrogen loadings. Volume expansions and formation energies are quantitatively similar to the average of fcc Ti and fcc Mg with weight factor of 0.25 and 0.75, respectively. Their values can be summarized as follows. (1) The volumes (normalized by the number of metal atoms in the unit cell) of three types of $Mg_{0.75}Ti_{0.25}H_2$ (24.36, 24.43, and 24.26 Å^3 for $ZrAl_3$ type, $TiAl_3$ type and $AuCu_3$ type, respectively) are larger than that of fluorite TiH_2 (21.09 Å^3) and smaller than that of fluorite MgH_2 (26.02 Å^3). (2) The energy difference between hydrogen in octahedral and tetrahedral sites is smaller in the alloys than in fcc Mg. For instance, hydrogen atoms occupying octahedral sites in $AuCu_3$ type alloy are 64 and 72 meV/H less stable than those in tetrahedral sites when H/M = 0.25 and H/M = 1, respectively. In addition, the formation energy of $AuCu_3$ type $Mg_{0.75}Ti_{0.25}H_2$ is the same to the average of fluorite TiH_2 and fluorite MgH_2 with weight factor of 0.25 and 0.75 (−0.63 eV/H_2). However 0.05, and 0.07 eV/H_2 lower formation energies than that of $AuCu_3$ type are found for $ZrAl_3$ type and $TiAl_3$ type, respectively. The comparison of stabilities of these three systems together with the segregated system will be further discussed later in this paper.

3.1.2. Segregated type

The formation energy of the segregated alloy (ΔE_{M}) is 0.04 eV/M, which is much lower than those of the other three alloys. Due to the different metal surroundings, four types of tetrahedral and three types of octahedral sites were found in the segregated type alloy. These are tetrahedral sites with four, two, one and zero Ti neighbors and octahedral sites with four, one and zero Ti neighbors. According to the type of sites and number of Ti neighbors, we name them $T(4Ti)$, $T(2Ti)$, $T(1Ti)$, $T(0Ti)$, $O(4Ti)$, $O(1Ti)$ and $O(0Ti)$, respectively. To determine the order of hydrogen loading in different sites, the formation energies of $Mg_{12}Ti_4H_1$ were calculated (see Table 1). The stability of hydrogen in these sites is in the order of $O(4Ti) > T(4Ti) > T(2Ti) > T(1Ti) > O(1Ti) > T(0Ti) > O(0Ti)$. This sequence of hydrogen loading into the alloy was followed when the formation energies as a function of hydrogen concentration were calculated. For instance, when hydrogen loads in the tetrahedral sites, the order of $T(4Ti)$, $T(2Ti)$, $T(1Ti)$ and $T(0Ti)$ has been followed; when hydrogen loads in octahedral sites, the order of $O(4Ti)$, $O(1Ti)$ and $Ti(0Ti)$ has been followed. When all of the tetrahedral sites are occupied, a concentration of H/M = 2 is obtained. However, when hydrogen loads in all of the octahedral sites, only a concentration of H/M = 1 can be achieved, and in order to get a concentration of H/M = 2, half of the tetrahedral sites needs to be further occupied (the sequence of $T(4Ti)$, $T(2Ti)$, $T(1Ti)$ and $T(0Ti)$ is again applied). The obtained formation energies are plotted in Fig. 2.

When hydrogen occupies tetrahedral sites, the formation energy decreases when H/M < 1; when H/M ≥ 1 the formation energy increases from −0.84 to −0.66 eV/H_2 with full hydrogen loading. When hydrogen atoms are stored in octahedral sites, the formation energy is very negative at low loading, e.g. when four $O(4Ti)$ sites are filled up to H/M = 0.25, the formation energy is −1.1 eV/H_2. Whereas when more hydrogen atoms are introduced, the formation energy increases except at concentration H/M = 1.25. This is related to the beginning of the storing hydrogen in $T(4Ti)$ sites after all the octahedral sites are occupied. When H/M > 1, the formation energies of hydrogen occupying a combination of

Table 1
Different interstitial sites in the segregated alloy and the formation energies of $Mg_{12}Ti_4H_1$. The energies are in eV/H_2. $N_{\mathrm{Ti-H}}$, N_T, and N_O represent number of Ti–H bonding and number of tetrahedral and octahedral sites, respectively.

$N_{\mathrm{Ti-H}}$	Tetrahedral sites	N_T	$\Delta E_{\mathrm{H_2}}$	Octahedral sites	N_O	$\Delta E_{\mathrm{H_2}}$
4	$T(4Ti)$	2	0.06	$O(4Ti)$	4	−0.16
2	$T(2Ti)$	10	0.35	–	–	–
1	$T(1Ti)$	6	0.62	$O(1Ti)$	8	0.77
0	$T(0Ti)$	14	1.58	$O(0Ti)$	4	1.74

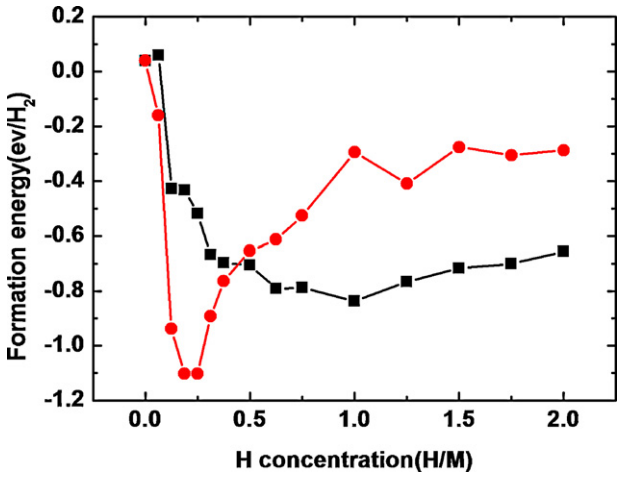

Fig. 2. Formation energies of hydrides ΔE_{H_2} as a function of hydrogen concentration in the segregated alloy. The stability sequence in Table 1 has been applied to load the alloy in tetrahedral (black curve) and octahedral sites (red curve), respectively. As there are only sixteen octahedral sites in the sixteen metal atoms cell, octahedral sites are occupied when $H/M \leq 1$, and another sixteen tetrahedral sites are occupied when $1 < H/M \leq 2$. (For interpretation of the references to color in this figure legend, the reader is referred to the web version of the article.)

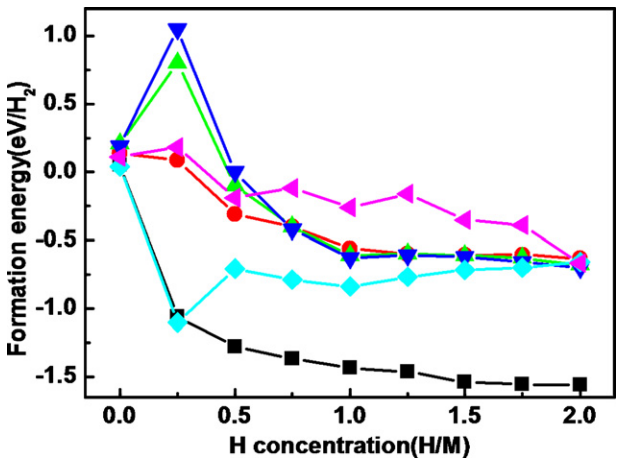

Fig. 3. Formation energies ΔE_{H_2} as a function of hydrogen concentration. The unit is eV/H_2. When H/M = 0, formation energies of alloys are in eV/M. Five structures including bct Mg (left triangles), $TiAl_3$ type (down triangles), $ZrAl_3$ type (up triangles), $AuCu_3$ type (circles) $Mg_{0.75}Ti_{0.25}$, segregated $Mg_{0.75}Ti_{0.25}$ (diamonds) and fcc Ti (squares) are presented. For the hydrides the lattice types of the metal atoms are specified. As the hydrogen atoms are at tetrahedral sites, fcc corresponds to a fluorite structure, while as the hydrogen atoms are at trigonal sites, bct corresponding to a rutile structure.

octahedral sites and tetrahedral sites are always higher than hydrogen only occupying tetrahedral sites. This is because the repulsive H–H interactions between hydrogen atoms occupying the nearest octahedral and tetrahedral sites in the Mg-rich region. For instance when half of hydrogen atoms occupy the octahedral sites and another half occupy tetrahedral sites, the H–H distance of 1.96 Å is smaller than the minimum H–H distance of 2.1 Å claimed by Westlake [49]. It should be mentioned that the Westlake criteria has some limitation as in some metal hydride, i.e. $RTInH_{1.333}$ (R = La, Ce, Pr, or Nd; T = Ni, Pd, or Pt) possess unusually short H–H separations [50]. To confirm this effect, formation energies of hydrogen atoms occupying combinations of $O(4Ti) + T(4Ti)$, $O(4Ti) + T(4Ti) + T(2Ti)$ have also been calculated. The calculated formation energies are always higher than the ones with hydrogen only occupying tetrahedral sites or only occupying octahedral sites. This is also due to the small H–H distance between the tetrahedral and octahedral sites at Ti-rich region. For instance, hydrogen occupying a combination of four $O(4Ti)$ and two $T(4Ti)$ sites leads to a higher formation energy of -0.58 eV/H_2 compared to those of hydrogen occupying only tetrahedral sites (-0.70 eV/H_2) and only octahedral sites (-0.76 eV/H_2). It should be noted that the total energy of the system ($E_{Mg_{0.75}Ti_{0.25}H_{2y}}$) always decreases with the increase of the hydrogen concentration.

Therefore, the most favorable hydrogenation process in Fig. 2 can be divided into three phases. (1) The $O(4Ti)$ and $O(1Ti)$ sites are favored in the low hydrogen concentration region when $H/M < 0.5$. When $H/M \geq 0.5$ the tetrahedral sites are always favored over octahedral sites. The hydrogen atoms already in the octahedral sites will be redistributed over the tetrahedral sites. (2) When $0.5 < H/M \leq 1.125$, the hydrogen atoms occupy $T(4Ti)$, $T(2Ti)$ and $T(1Ti)$ sites. (3) When $1.125 < H/M < 2$, the hydrogen atoms start loading into the $T(0Ti)$ sites. When H/M = 2, the hydrogen atoms are occupying all tetrahedral sites. The hydrogenation energies will be compared with those of pure Ti and Mg in the following sections.

3.2. Comparison of hydrogenation properties between $Mg_{0.75}Ti_{0.25}$ alloys, Mg and Ti

The formation energies as a function of hydrogen concentration with respect to six different structures, including Mg, $ZrAl_3$ type, $TiAl_3$ type, $AuCu_3$ type, segregated type $Mg_{0.75}Ti_{0.25}$ alloys, and Ti are plotted in Fig. 3. Structural information and formation energies are summarized in 1. When H/M = 0, the formation energies are the energy cost of converting hcp metals into the structures which are the same as those of the corresponding hydrides. For instance, the energy cost of converting hcp Mg to bct Mg is 0.11 eV/M. As shown, the energy costs for creating the segregated type, and $ZrAl_3$ type $Mg_{0.75}Ti_{0.25}$ alloy are the lowest (0.04 eV/M), and the highest (0.21 eV/M), respectively. For those of $AuCu_3$ type, $TiAl_3$ type, the energies are 0.14, and 0.19 eV/M, respectively. The relatively high energies of the three ordered alloys are in line with the prediction that Mg and Ti are immiscible. In fact, the calculated enthalpy of mixing Mg and Ti metals to the $ZrAl_3$ type alloy are very similar to that of $Mg_{0.50}Ti_{0.50}$ (0.21 eV/M) [47].

With full loading of hydrogen, the stability of these four hydride systems is $TiAl_3$ type > $ZrAl_3$ type > segregated type > $AuCu_3$ type. $TiAl_3$ type $Mg_{0.75}Ti_{0.25}H_2$ is 0.07, and 0.04 eV/H_2 more stable than the $AuCu_3$ type and segregated type, respectively. The most negative formation energy of $TiAl_3$ type $Mg_{0.75}Ti_{0.25}H_2$ is probably due to the smallest Ti–H bond length of 1.92 Å in the four structures. However, the stability sequence of the hydrides is not consistent with the stability sequence of the alloy systems where segregated type > $AuCu_3$ type > $TiAl_3$ type > $ZrAl_3$ type. The different stability sequences of the alloys and hydrides indicates hydrogen induced structural transformation upon hydrogen cycling.

As shown in Fig. 3 when hydrogen atoms are stored in the metals, the formation energies change very differently. The five systems can be seen as three groups:

(1) The $AuCu_3$ type, $TiAl_3$ type, $ZrAl_3$ type $Mg_{0.75}Ti_{0.25}$ alloys have similar hydrogenation properties as Mg. Therefore we can denote these as Mg-like structures. In these materials octahedral sites are never favored and hydrogen atoms prefer to occupy tetrahedral sites which are close to each other. In Mg, an odd number of hydrogen atom always corresponds to an increase in the energy, and coupling of two hydrogen atoms is necessary to make the hydride stable [41]. For $ZrAl_3$ type, $TiAl_3$ type and $AuCu_3$ type systems, an odd number of hydrogen atoms does not cause the formation energy to increase, but hydrogen atoms occupying sites close to each other are more stable than occupying sites far apart. The formation energies of hydrides at low hydrogen loading are positive but generally

Table 2
Formation energies, structures and bonds of the rutile MgH_2, fluorite TiH_2 and four types of $Mg_{0.75}Ti_{0.25}H_2$ shown in Fig. 1. ΔE_M (in eV/M) is the energy cost of converting hcp metals to bct, fcc metals and alloys. ΔE_{H_2} (in eV/H_2) are formation energies of hydrides. Parameters are in Å, and volumes are in Å^3. Mg–H and Ti–H in segregated $Mg_{12}Ti_4H_{32}$ are the distances between metal and hydrogen, where the hydrogen atom is in the tetrahedral site with only Mg or only Ti surroundings. In rutile MgH_2, hydrogen atoms are displaced from the ideal trigonal sites and two different Mg–H bond lengths were observed.

	MgH_2	$TiAl_3$	$ZrAl_3$	$AuCu_3$	Segregated	TiH_2
ΔE_M	0.11	0.19	0.21	0.14	0.04	0.05
ΔE_{H_2}	−0.67	−0.70	−0.68	−0.63	−0.66	−1.55
$\Delta E_{H_2} - \Delta E_M$	−0.78	−0.89	−0.89	−0.77	−0.70	−1.60
Parameters	*a*(4.45)	*a*(4.57)	*a*(4.59)	*a*(4.59)	*a*(9.24)	*a*(4.40)
	c(2.99)	*c*(9.27)	*c*(18.53)		*c*(4.57)	
Volume	59.42	194.72	389.75	97.02	389.92	84.93
H–H	2.73	2.20, 2.26	2.26, 2.35	2.23, 2.36	2.23, 2.30	2.20
Mg–H	1.94, 1.92	2.01	2.01	2.01	2.02	–
Ti–H	–	1.92	1.93	1.93	1.94	1.90

decrease with increasing hydrogen concentration and converge at around −0.70 eV/H_2 with full hydrogen loadings.

(2) For fcc Ti, octahedral sites are favored when H/M ≤ 0.25; tetrahedral sites are favored when H/M > 0.25. The behavior of hydrogen clustering which is found in Mg-like structures is absent. The formation energies are much more negative than those of the Mg-like metals, for example −1.06 and −1.55 eV/H_2 for concentrations of H/M = 0.25 and 2, respectively.

(3) For the segregated $Mg_{0.75}Ti_{0.25}$ alloy, at low hydrogen concentration when H/M ≤ 0.25, hydrogen atoms load in the Ti-rich region, so the hydrogenation properties are more Ti-like. After the favorable octahedral sites of the Ti-rich regions are occupied, the hydrogen atoms start loading in the Ti–Mg coherent region when 0.25 < H/M ≤ 1.125, and the hydrogenation properties are similar to those of the ordered $Mg_{0.75}Ti_{0.25}$ alloys. When H/M > 1.125, the Mg-rich region starts absorbing hydrogen, making this part of process more Mg-like. The formation energy decreases dramatically in the Ti-rich region and the formation energy curve has a high negative value of −1.10 eV/H_2 at H/M = 0.25. After that hydrogen atoms start loading in Mg–Ti coherent region, the formation energy increases to −0.70 eV/H_2 at H/M = 0.5, and another minimum −0.82 eV/H_2 can be found at H/M = 1.0. When H/M > 1.125 (hydrogen is stored in the Mg-rich region), the formation energy increases towards the same value as that of rutile MgH_2 with full hydrogen loading.

4. Discussion

4.1. Electronic structures

Because Ti–H bonding is much stronger than that of Mg–H, one would expect that the formation energies of $Mg_{0.75}Ti_{0.25}H_2$ hydrides are much more negative than that of rutile MgH_2. However, all the calculated hydrides have similar energies to that of rutile MgH_2 (see Fig. 3). How does Ti affect the structural and electronic bonding properties of the hydrides? To understand this question, the structures and electron density of states (DOS) of these six hydrides are analyzed and shown in Table 2 and Fig. 4, respectively. As important point should be mentioned that in alloys hydrogen atoms do not occupy the ideal interstitial sites, but are displaced to a point where hydrogen atoms are closer to Ti than Mg. For instance, the distance between Mg and H is larger than that of Ti and H in ordered $Mg_{0.75}Ti_{0.25}H_2$. In the Ti and Mg coherent region in $Mg_{12}Ti_4H_{32}$, hydrogen atoms are also displaced closer to Ti atoms. However, despite the shortening, the Ti–H bond lengths in alloy hydrides are still larger than that in the fluorite TiH_2, which is due to the larger volume of the $Mg_{0.75}Ti_{0.25}H_2$ compared to TiH_2. Mg–H bond lengths in the alloy hydrides are also larger than that in rutile MgH_2. The origin for the longer Mg–H bond is mainly due to the structure rearrangement of Mg from bct to fcc, while the longer Ti–H bond is mainly caused by the lattice expansion due to the inclusion of Mg.

To confirm the effect of alloying Mg with Ti, the total DOSs of the hydrides and the partial DOSs of Mg, Ti and H atoms were calculated and the results are plotted in Fig. 4. A large band gap around the Fermi level is observed in rutile MgH_2. The valence bands are primarily determined by mixing hydrogen 1s and Mg 3s states in the peak at the lowest energy; whereas the second peak which is close to the Fermi level is composed mainly of mixing hydrogen 1s and Mg orbital with 2p character. The conduction bands have significant unoccupied Mg 3s and 2p characters with a very small amount of unoccupied hydrogen 1s states. These indicate that the bonding in rutile MgH_2 is dominantly ionic. This agrees with the results of Vajeeston et al. [48]. In contrast, covalent bonding properties are found in fluorite TiH_2. Two peaks in both the valence and conduction bands with consecutive states around the Fermi level can be seen in fluorite TiH_2. The valence bands consist of mainly hydrogen 1s states, a small amount of Ti 3p and some of Ti 3d states. The majority of Ti 3d states lie between −2.5 and 2.5 eV. For the partial DOS of the hydrogen atom, two sharp peaks can be seen between −5 and −5.5 eV in the valence bands, whereas hardly any hydrogen state is contributing to the conduction bands.

For those four types of $Mg_{0.75}Ti_{0.25}H_2$, the DOSs are clearly different from those of rutile MgH_2 and fluorite TiH_2. Very similar properties of DOSs can be found except those of the three ordered structures are more spread out than the segregated one. They can be characterized by (i) the large band gap which was found in the total DOS of rutile MgH_2 is absent; (ii) a structure at low energy, which is centered at around −5 eV below the Fermi level, consisting mainly of Ti 3d and hydrogen 1s and a weaker Mg sp hybridization, and (iii) the bonding peak near the Fermi level is dominated by the stronger Ti–H, H–H, and weaker Mg–H interaction. In addition, the Fermi level of $ZrAl_3$ type, $TiAl_3$ type, $AuCu_3$ type and segregated $Mg_{0.75}Ti_{0.25}H_2$ are 4.2, 4.3, 4.4 and 4.0 eV, respectively. These value are both larger than that of rutile MgH_2 (0.2 eV) and smaller than that of fluorite TiH_2 (5.8 eV). The shift of the Fermi level leads to a reduction of the stability of Mg–H bonding compared with that of rutile MgH_2. On the other hand, the Ti 3d and the hydrogen 1s states are both broadened and shifted to higher energy compared with that of fluorite TiH_2, and the delocalization suggests weaker Ti–H bonding in the alloy hydrides. The weakening of both Mg–H and Ti–H bonding is in line with our prediction of the structure analyse.

4.2. Reversibility of (de)hydrogenation of $Mg_{0.75}Ti_{0.25}$

Besides the thermodynamic and kinetics, the reversibility is also a very important issue for hydrogen storage materials. As already analyzed, the segregated type and $TiAl_3$ type structures are favored for the alloys and the hydrides, respectively. This means that hydrogen induced structural rearrangement of the intermetallic

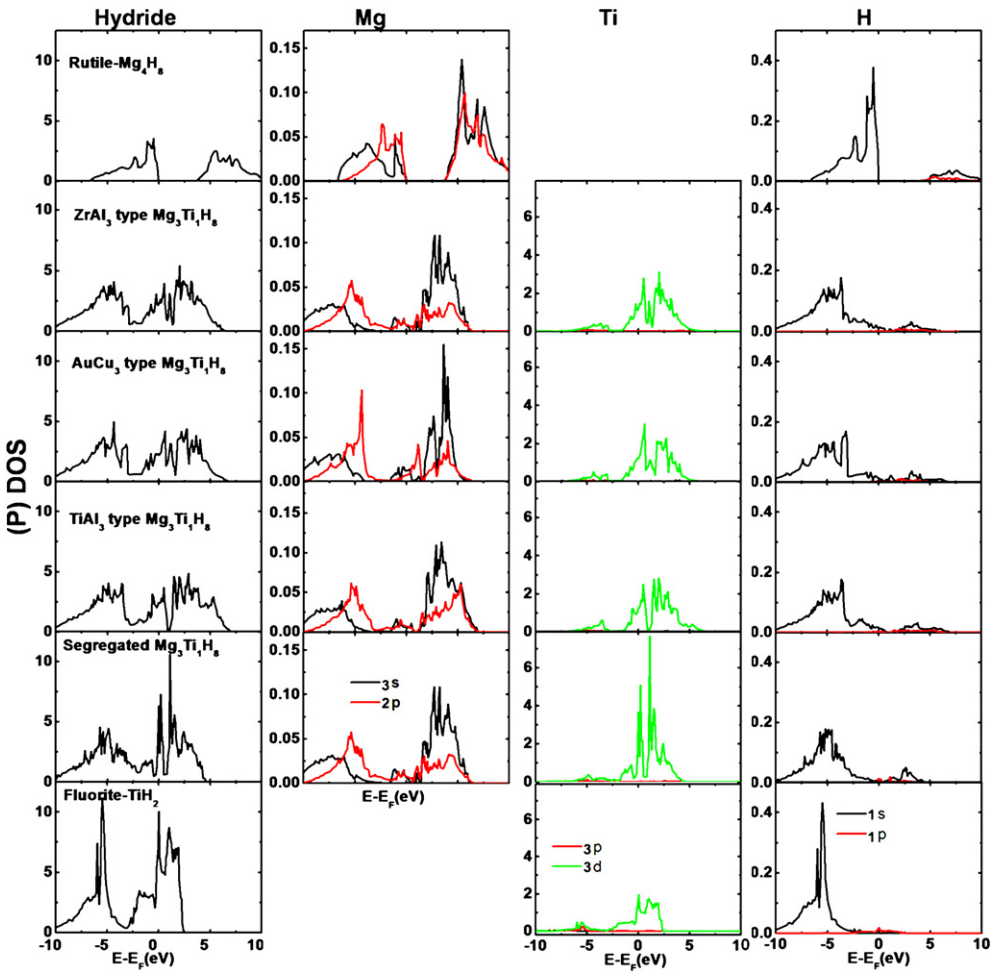

Fig. 4. Total and partial DOSs of the hydrides. From left to right are the total DOS of the hydrides, PDOSs of Mg, Ti and H atoms in the hydrides. From top to bottom are rutile MgH_2, fluorite MgH_2, mixed $Mg_{0.75}Ti_{0.25}H_2$, segregated $Mg_{0.75}Ti_{0.25}H_2$, and fluorite TiH_2. The PDOS of hydrogen in the segregated $Mg_{0.75}Ti_{0.25}H_2$ is the one which is in the tetrahedral site in Mg–Ti coherent region. For the DOSs of hydrides four metal atoms cell are used and the unit is states/atom eV; for the PDOSs of the atoms, the unit is states/atom eV.

structures of the $Mg_{0.75}Ti_{0.25}$ might occur upon hydrogen cycling, i.e. segregated alloy transforms to $TiAl_3$ type hydride upon hydrogenation and reverse transformation upon dehydrogenation. In fact, for $InPd_3$ alloys, hydrogen induced structural transformations from $TiAl_3$ type and $ZrAl_3$ type alloys to $AuCu_3$ type hydride have been observed experimentally [51,52]. However, $TiAl_3$ type $Mg_{0.75}Ti_{0.25}H_2$ and the hydrogen induced structure transformation between $TiAl_3$ type and $AuCu_3$ type or segregated type of structures has not been reported yet. This is probably due to the different Mg/Ti ratio used, also probably because that the homogenous Mg–Ti alloys or Mg–Ti–H have never been successfully prepared experimentally. In addition, the formation of the stable $TiAl_3$ type $Mg_{0.75}Ti_{0.25}H_2$ compound indicate that inclusion of TiH_2 into MgH_2 is more feasible rather than adding Ti into Mg metals. The hydrogen storage properties can be optimized by using different approaches and different composition of the materials.

The reality is that homogenous Mg–Ti alloys have never been successfully prepared, whereas various structures including thin film and bulk alloys with partial or nano-sized segregation of Ti in Mg were found in the products. Within these structures, the demixing effect might bring in more segregation regions or even complete segregation upon running the hydrogen cycles. It can be noticed that in Table 2, all the ordered and segregated fluorite structures are less stable than the combination of rutile MgH_2 and fluorite TiH_2. Therefore if enough thermal activation for atomic rearrangement is allowed, one would expect complete phase separation during hydrogen cycling. To search for solutions we would like to refer to Fig. 3. The formation energy curve of hydrogen concentration from 2 to 0 corresponds to dehydrogenation. During the dehydrogenation, there is a driving force to form Ti segregation due to the low formation energy of the segregated alloy. However if we take a look at the Ti-rich region in the segregated structure, even with a little amount of hydrogen retained in the alloys after dehydrogenation, the formation energy is still very negative. This part of hydrogen can only desorb at higher temperatures than the hydrogen atoms occupying Mg-rich region. This allows the possibility of partial dehydrogenation process and the trapped hydrogen in Ti-rich region might help to maintain the original structure of the alloys rather than demix to form larger scale of Ti segregation. Therefore the reversibility can be improved by regulating the dehydrogenation process with a low-bound for the hydrogen content. At this point, it should be pointed out that the prediction of the demixing scale is beyond the ability of the current DFT studies due to limited computational time. Future molecular dynamic investigations are necessary in the future.

5. Conclusions

Formation energies of hydrogen absorbing in $Mg_{0.75}Ti_{0.25}$ alloys as a function of the hydrogen concentration were calculated using the Density Functional Theory. Energies and structures were analyzed and compared with those of pure Mg and Ti. The structural

transformation from rutile to fluorite is achieved by alloying Mg with 25 at.% Ti. The hydrogenation properties depend highly on the structure of the alloys. The ordered alloys behave very similarly to pure Mg. For the segregated alloy, Ti-rich, Mg–Ti coherent and Mg-rich regions are found. The hydrogenation process can be divided into three parts from low to high hydrogen concentration, and these are Ti-like, ordered alloy-like and Mg-like, respectively. The DOSs of the hydrides were examined and relate with the formation energies. In $Mg_{0.75}Ti_{0.25}H_2$, Mg–H and Ti–H bonds are weakened compared with that of fluorite TiH_2 and that of rutile MgH_2. The weaker Mg–H bonding is mainly caused by the rearrangement of the metal lattice from bct to fcc. The weaker Ti–H bonding is due to the expansion of the lattice because of the inclusion of Mg metal. From the thermodynamic point of view, the segregated structure is favored for alloy, whereas a stable $TiAl_3$ type $Mg_{0.75}Ti_{0.25}H_{2y}$ is favored for hydride. Therefore, hydrogen induced structure transformation between $TiAl_3$ type and segregated type of structures might occur upon hydrogen cycling. In addition, for non-homogenous Mg–Ti–H system further segregation of Ti in Mg might occur. It is not favorable for the reversibility of this system. Partial dehydrogenation might be the solution to improve the reversibility of this system.

References

[1] L. Schlapbach, A. Züttel, Nature 414 (2001) 353.
[2] B. Bogdanovic, H. Hofmann, A. Neuy, A. Reiser, K. Schlichte, B. Spliethoff, S. Wessel, J. Alloys Compd. 292 (1999) 57.
[3] B. Bogdanovic, Int. J. Hydrogen Energy 9 (1984) 937.
[4] G. Liang, J. Huot, S. Boily, A.V. Neste, R. Schulz, J. Alloys Compd. 291 (1999) 295.
[5] G. Liang, J. Alloys Compd. 370 (2004) 123.
[6] M.Y. Song, D.R. Mumm, S.N. Kwon, S.H. Hong, J.S. Bae, J. Alloys Compd. 416 (2006) 239.
[7] H. Reule, M. Hirscher, A. Weisshardt, H. Kronmuller, J. Alloys Compd. 305 (2000) 246.
[8] Z. Dehouche, J. Goyette, T.K. Bose, J. Huot, R. Schulz, Nano Lett. 1 (2001) 175.
[9] J.F.R. De Castro, S.F. Santos, A.L.M. Costa, A.R. Yavari, W.J. Botta, T.T. Ishikawa, J. Alloys Compd. 376 (2004) 251.
[10] J. Charbonnier, P. de Rango, D. Fruchart, S. Miraglia, L. Pontonnier, S. Rivoirard, N. Skryabina, P. Vulliet, J. Alloys Compd. 383 (2004) 205.
[11] N. Hanada, T. Ichikawa, H. Fujii, J. Phys. Chem. B 109 (2005) 7188.
[12] G. Barkhordarian, T. Klassen, R. Bormann, J. Phys. Chem. B 110 (2006) 11020.
[13] T. Vegge, L.S. Hedegaard-Jensen, J. Bonde, T.R. Munter, J.K. Nørskov, J. Alloys Compd. 386 (2005) 1.
[14] A.J. Du, S.C. Smith, X.D. Yao, G.Q. Lu, J. Phys. Chem. B 109 (2005) 18037.
[15] A.J. Du, S.C. Smith, X.D. Yao, G.Q. Lu, J. Phys. Chem. B 110 (2006) 21747.
[16] Y. Song, Z.X. Guo, R. Yang, R. Mater. Sci. Eng. A 365 (2004) 73.
[17] W.P. Kalisvaart, H.J. Wondergem, F. Bakker, P.H.L. Notten, J. Mater. Res. 22 (2007) 1640.
[18] W.P. Kalisvaart, P.H.L. Notten, J. Mater. Res. 23 (2008) 2179.
[19] R.A.H. Niessen, P.H.L. Notten, Electrochem. Solid-State Lett. 8 (2005) A534.
[20] P. Vermeulen, R.A.H. Niessen, P.H.L. Notten, Electrochem. Commun. 8 (2006) 27.
[21] D.M. Borsa, A. Baldi, M. Pasturel, H. Schreuders, B. Dam, R. Griessen, P. Vermeulen, P.H.L. Notten, Appl. Phys. Lett. 88 (2006) 241910.
[22] M. Slaman, B. Dam, M. Pasturel, D.M. Borsa, H. Schreuders, J.H. Rector, R. Griessen, Sens. Actuators B 123 (2007) 538.
[23] D.M. Borsa, R. Gremaud, A. Baldi, H. Schreuders, J.H. Rector, B. Kooi, P. Vermeulen, P.H.L. Notten, B. Dam, R. Griessen, Phys. Rev. B 75 (2007) 205408.
[24] A. Baldi, D.M. Borsa, H. Schreuders, J.H. Rector, T. Atmakidis, M. Bakker, Int. J. Hydrogen Energy 33 (2008) 3188.
[25] G. Liang, J. Huot, S. Boily, A. Van Neste, R. Schulz, J. Alloys Compd. 292 (1999) 247.
[26] G. Liang, J. Huot, S. Boily, A. Van Neste, R. Schulz, J. Alloys Compd. 282 (1999) 286.
[27] G. Liang, R. Schulz, J. Mater. Sci. 38 (2003) 1179.
[28] T. Mitchell, S. Diplas, P. Tsakiropoulos, J.F. Watts, J.A.D. Matthew, Philos. Mag. A 82 (2002) 841.
[29] P. Vermeulen, R.A.H. Niessen, D.M. Borsa, B. Dam, R. Griessen, P.H.L. Notten, Electrochem. Solid-State Lett. 9 (2006) A520.
[30] B. Zahiri, C.T. Harrower, B. Shalchi-Amirkhiz, D. Mitlin, Appl. Phys. Lett. 95 (2009) 103114.
[31] X. Tan, C.T. Harrower, B. Shalchi-Amirkhiz, D. Mitlin, Int. J. Hydrogen Energy 34 (2009) 7741.
[32] P. Vermeulen, P.C.J. Graat, H.J. Wondergem, P.H.L. Notten, Int. J. Hydrogen Energy 33 (2008) 5646.
[33] B.R. Pauw, W.P. Kalisvaart, S.X. Tao, M.T.M. Koper, A.P.J. Jansen, P.H.L. Notten, Acta Mater. 56 (2008) 2948.
[34] S. Er, D. Tiwari, G.A. de Wijs, G. Brocks, Phys. Rev. B 79 (2009) 024105.
[35] P. Vermeulen, H.J. Wondergem, P.C.J. Graat, D.M. Borsa, H. Schreuders, B. Dam, R. Griessen, P.H.L. Notten, J. Mater. Chem. 18 (2008) 3680.
[36] S. Srinivasan, P.C.M.M. Magusin, W.P. Kalisvaart, P.H.L. Notten, F. Cuevas, M. Latroche, R.A. van Santen, Phys. Rev. B 81 (2010) 054107.
[37] A. Baldi, R. Gremaud, D.M. Borsa, C.P. Baldé, A.M.J. van der Eerden, G.L. Kruijtzer, P.E. de Jongh, B. Dam, R. Griessen, Int. J. Hydrogen Energy 34 (2009) 1450.
[38] Y. Choi, J. Lu, H.Y. Sohn, Z.Z. Fang, J. Power Sources 180 (2008) 491.
[39] Y. Choi, J. Lu, H.Y. Sohn, Z.Z. Fang, E. Rönnebro, J. Phys. Chem. C 180 (2009) 19344.
[40] J. Lu, Y. Choi, Z.Z. Fang, H.Y. Sohn, E. Rönnebro, J. Am. Chem. Soc. 131 (2009) 15843.
[41] S.X. Tao, P.H.L. Notten, R.A. van Santen, A.P.J. Jansen, Phys. Rev. B 79 (2009) 144121.
[42] G. Kresse, J. Furthmüller, Phys. Rev. B 54 (1996) 11169.
[43] G. Kresse, J. Furthmüller, J. Comp. Mater. Sci. 6 (1996) 15.
[44] G. Kresse, D. Joubert, Phys. Rev. B 59 (1999) 1758.
[45] J.P. Perdew, J. Phys.: Condens. Matter 172 (1991) 1.
[46] H.J. Monkhorst, J.D. Pack, Phys. Rev. B 13 (1976) 5188.
[47] F.R. de Boer, R. Boom, W.C.M. Mattens, A.R. Miedema, A.K. Niessen, Cohesion in Metals: Transition Metal Alloys, North-Holland, Amsterdam, 1988.
[48] P. Vajeeston, P. Ravindran, B.C. Hauback, H. Fjellvåg, A. Kjekshus, S. Furuseth, M. Hanfland, Phys. Rev. B 73 (2006) 224102.
[49] (a) D.G. Westlake, J. Less Common Met. 75 (1980) 177;
(b) D.G. Westlake, J. Less Common Met. 90 (1983) 251;
(c) D.G. Westlake, J. Less Common Met. 91 (1983) 275.
[50] P. Ravindran, P. Vajeeston, B.C. Hauback, H. Fjellvåg, Phys. Rev. Lett. 89 (2002) 106403.
[51] H. Kohlmann, J. Solid State Chem. 183 (2010) 367.
[52] H. Kohlmann, C. Ritter, Z. Anorg. Allg. Chem. 635 (2009) 1573.